PAPER

A High-Resolution Imaging Algorithm without Derivatives Based on Waveform Estimation for UWB Radars

Shouhei KIDERA[†a)], ***Student Member***, **Takuya SAKAMOTO**[†], ***Member***, ***and*** **Toru SATO**[†], ***Fellow***

SUMMARY UWB pulse radars enable us to measure a target location with high range-resolution, and so are applicable for measurement systems for robots and automobile. We have already proposed a robust and fast imaging algorithm with an envelope of circles, which is suitable for these applications. In this method, we determine time delays from received signals with the matched filter for a transmitted waveform. However, scattered waveforms are different from transmitted one depending on the target shape. Therefore, the resolution of the target edges deteriorates due to these waveform distortions. In this paper, a high-resolution imaging algorithm for convex targets is proposed by iteration of the shape and waveform estimation. We show application examples with numerical simulations and experiments, and confirm its capability to detect edges of an object.

key words: *UWB pulse radars, fast and robust radar imaging, inverse problem, high resolution imaging, edge detection*

1. Introduction

UWB pulse radars are attractive for high-resolution imaging, which is required for measuring techniques of robots. They can also be applied to a non-destructive measurement for surface details of the antennas and the aircrafts, because it is needed to detect small surface defects. These applications require a fast, robust, and high-resolution imaging technique. However, the conventional imaging algorithms require an intensive computation [1]–[4]. For these applications, we have already proposed SEABED [5], [6]. This method utilizes a reversible transform BST (Boundary Scattering Transform) between the time delay and the target boundary to achieve fast and direct target imaging. However, the estimated image is unstable in a noisy environment because it utilizes the derivative of received data. To resolve this problem, we have proposed a robust and fast imaging algorithm with an envelope of circles [7]. This method utilizes the principle that the target boundaries are expressed as the envelopes of the circles with the radius of the time delays. Our method can realize robust imaging even in a noisy environment. However, the accuracy is at least about 1/10 of the center wavelength of the pulse because the image is distorted especially around sharp edges. This is due to the assumption that the scattered waveform is the same as the transmitted one. In general, the cost of the lower-frequency component is low compared to that of the higher-frequency one. This is a reason why we need to enhance the accuracy of the image.

This paper proposes a shape estimation method with a waveform estimation in order to enhance the resolution of the image. An imaging algorithm based on this idea has been published [8]. However, the earlier study utilizes a parametric approach and can be applied only to a simple polygon. In this paper, we extend this idea to general convex targets including smooth curves and edges. Numerical simulations and experiments show that the proposed method accomplishes a high-resolution imaging.

2. System Model

This paper deals with 2-dimensional problems and TE mode waves. It assumes that the target has a convex shape, and surrounded by a clear boundary which is composed of smooth curves concatenated at discrete edges. It assumes that the propagation speed of the radiowave is constant and known. We utilize a mono-static radar system. The induced current at the transmitting antenna is a mono-cycle pulse. The lower side of Fig. 1 shows the system model.

R-space is defined as the real space where the target

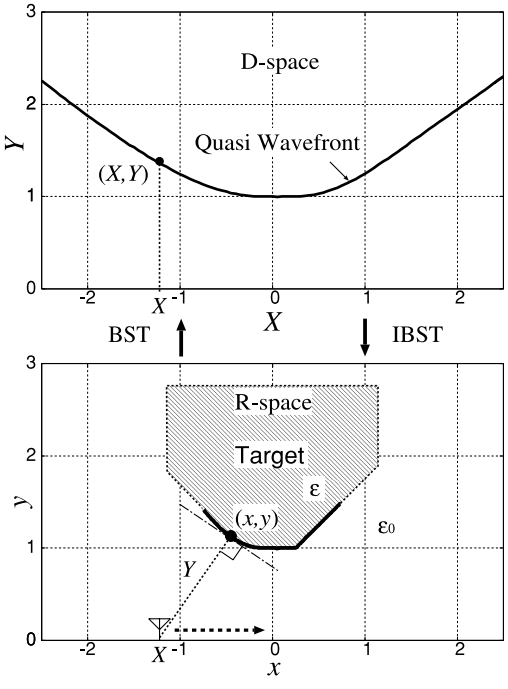

Fig. 1 D-space (Upper) and R-space (Lower) in the system model.

Manuscript received October 20, 2006.
Manuscript revised January 12, 2007.

[†]The authors are with the Department of Communications and Computer Engineering, Graduate School of Informatics, Kyoto University, Kyoto-shi, 606-8501 Japan.
a) E-mail: kidera@aso.cce.i.kyoto-u.ac.jp

DOI: 10.1093/ietcom/e90–b.6.1487

and the antenna are located. R-space is expressed with the parameters (x, y). An omni-directional antenna is scanned along x axis. Both x and y are normalized by λ, which is the center wavelength of the transmitted pulse. It assumes $y > 0$ for simplicity. $s'(X, Y)$ is defined as the electric field received at the antenna location $(x, y) = (X, 0)$, where Y is defined with the arrival time t of the echo and the speed of the radio wave c as $Y = ct/(2\lambda)$. The matched filter is applied with the transmitted waveform to $s'(X, Y)$. $s(X, Y)$ is defined as the output of the filter. D-space is defined as the space expressed by (X, Y), and we call it a quasi wavefront. The transform from (X, Y) to (x, y) corresponds to imaging which we deal with in this paper.

3. Conventional Method

In this section, we explain the conventional imaging algorithm with an envelope of circles. It has been already revealed that there is a reversible transform between a point on the target boundary (x, y) and a point on the quasi wavefront (X, Y) in SEABED [5]. This transform is named as BST (Boundary Scattering Transform). BST and IBST (Inverse BST) are expressed as

$$\left.\begin{aligned} X &= x + y\mathrm{d}y/\mathrm{d}x \\ Y &= y\sqrt{1 + (\mathrm{d}y/\mathrm{d}x)^2} \end{aligned}\right\}, \tag{1}$$

$$\left.\begin{aligned} x &= X - Y\mathrm{d}Y/\mathrm{d}X \\ y &= Y\sqrt{1 - (\mathrm{d}Y/\mathrm{d}X)^2} \end{aligned}\right\}. \tag{2}$$

Figure 1 shows the relationship between D-space and R-space. It has been proved that points on the target boundary should be expressed as points on the envelope of circles with the radius of Y and the center $(X, 0)$ for the quasi wavefront. Figure 2 shows the relationship between a quasi wavefront and an envelope of circles. This relationship enables us to estimate the convex targets including edges with the following procedure [7].

Step 1). Apply the matched filter to the received signals $s'(X, Y)$ and obtain the output $s(X, Y)$.

Step 2). Extract a quasi wavefront as (X, Y) by connecting the peak of $s(X, Y)$.

Step 3). Calculate the estimated shape $y = \max_X \sqrt{Y^2 - (x - X)^2}$ for each x.

Figure 3 presents the applied example with the conventional method. The image is distorted, and target boundaries cannot be correctly identified. The error around the edges is approximately 0.07λ. This is because of the waveform distortion, which is not negligible around the edges.

4. Proposed Method

4.1 Scattered Waveform Estimation

In this section, we propose an imaging algorithm with

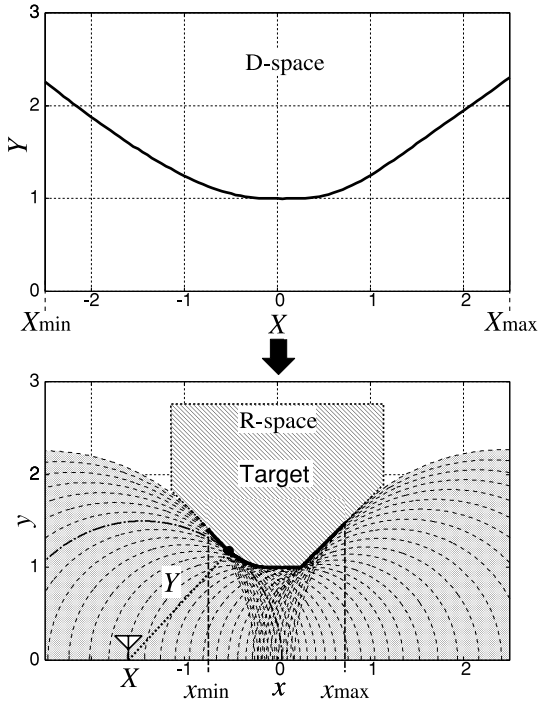

Fig. 2 Quasi wavefront in D-space (Upper) and an envelope of circles in R-space (Lower).

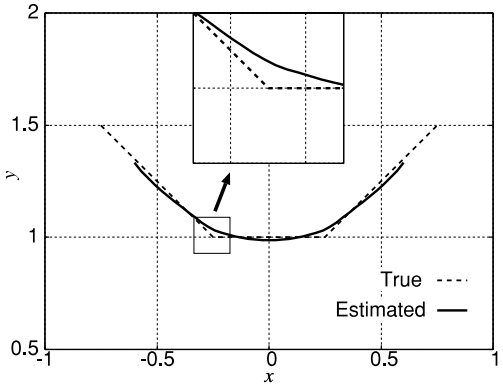

Fig. 3 Estimated image with the conventional method.

scattered waveform estimation. We iterate the shape and waveform estimation to the observed data by updating the matched filter. There are many algorithms to calculate scattered waveforms, such as FDTD (Finite Difference Time Domain) method and Moment Method in order to estimate scattered waveforms. However these methods require an intensive computation, which spoil the advantage of the quick imaging of our method. We have already proposed a fast scattered waveform estimation for a finite plain boundary in the 2-dimensional problems [8]. This method is based on the integral of Green's function along the boundary, and can be readily extended to the general convex target as follows. Figure 4 illustrates the antenna location and the target boundary. The transfer function is calculated with the integral of the Green's function along target boundaries which

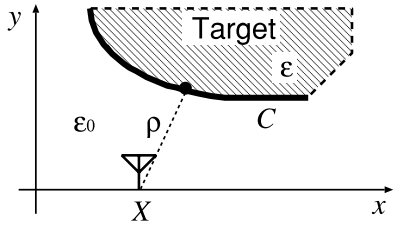

Fig. 4 Arrangement of the antenna and the convex target.

dominantly contribute to the scattering. The scattered waveform $F(\omega)$ in the frequency domain is approximated as

$$F(\omega) = \sqrt{\frac{\mathrm{j}k}{2\pi}} E_0(\omega) \int_C g(2\rho)\, \mathrm{d}s, \tag{3}$$

where C is the integration path, ρ is the distance between the antenna and the target boundary, k is the wavenumber, $E_0(\omega)$ is the transmitted waveform in the frequency domain, and g is the 2-dimensional Green's function, which is expressed as the 0th order Hankel's function of the 2nd kind. Although this method is not a strict solution for the scattered waveforms, the accuracy is sufficient for our application.

4.2 Procedure of the Proposed Method

The actual procedure of the proposed method is explained as follows. $X_{\min}$ and $X_{\max}$ as the minimum and the maximum X are defined as shown in Fig. 2. We define the target boundary and the quasi wavefronts as C_0 and $Y_0(X)$, respectively, which are estimated with the conventional method.

Step A). Estimate an initial target boundary with the conventional method. Set $i = 1$, where i is the iteration number.

Step B). Calculate the waveform for each X as

$$F_i(X, \omega) = \sqrt{\frac{\mathrm{j}k}{2\pi}} E_0(\omega) \int_{C_{i-1}} g(2\rho)\mathrm{d}s. \tag{4}$$

where C_{i-1} is the estimated boundary for $i-1$ th iteration.

Step C). Update the output of the matched filter as

$$s_i(X, Y) = \int_{-\infty}^{\infty} S'(X, \omega) F_i(X, \omega)^* \mathrm{e}^{\mathrm{j}\omega 2Y} \mathrm{d}\omega, \tag{5}$$

where $S'(X, \omega)$ is the received signal in the frequency domain. Extract the quasi wavefront for i th iteration as

$$Y_i(X) = \arg\max_Y s_i(X, Y). \tag{6}$$

Step D). Evaluate the updated quasi wavefront with the evaluation value ΔQ_i defined as

$$\Delta Q_i = \frac{\int_{X_{\min}}^{X_{\max}} |Y_i(X) - Y_{i-1}(X)|\, \mathrm{d}X}{\int_{X_{\max}}^{X_{\min}} \mathrm{d}X}. \tag{7}$$

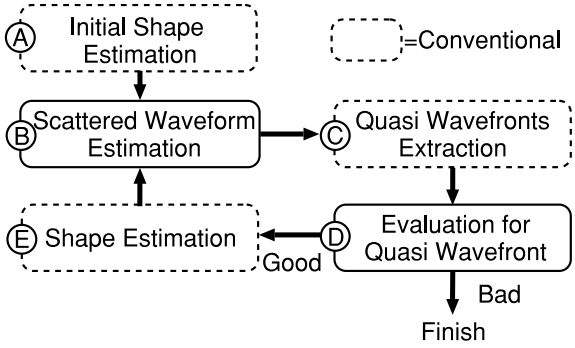

Fig. 5 Flowchart of the proposed method.

Step E). The following equation is applied

$$\Delta Q_i < \begin{cases} \epsilon & (i = 1), \\ \Delta Q_{i-1} & (i \geq 2). \end{cases} \tag{8}$$

If the equation holds true, we update the target boundary $(x, y) \in C_i$ as

$$y = \max_X \sqrt{Y_i(X)^2 - (x - X)^2}, \tag{9}$$

set $i = i + 1$, and return to the Step B). Otherwise, we complete the shape estimation. ϵ is set empirically.

For successive iteration, ΔQ_i is assume to become smaller, and Step E.) prevents the incorrect divergence of the estimated image with the iteration. By this procedure, the estimated waveform approaches to the true one. This improvement can enhance the resolution of the target shape. Figure 5 shows the flowchart of the proposed method.

5. Performance Evaluation

5.1 Examples of Waveform Estimation for Convex Targets

First, examples of the waveform estimation are presented to evaluate the accuracy for the estimated quasi wavefront of the convex target. Figures 6 and 7 show the error of the quasi wavefront for each antenna location with the matched filter for the transmitted and estimated waveform, respectively. The accuracy of the quasi wavefront with the estimated waveform is within 0.01λ/c around the edges. This level of accuracy cannot be obtained with the conventional filter. Also the waveform estimation is effective for any antenna location except for the upper left side of Fig. 7. In this region, the upper side of the target boundary strongly contributes the scattered waveform, which is a shadow region of Eq. (3). Additionally, Fig. 8 shows the transmitted and estimated waveform at the antenna location at $(x, y) = (4.0\lambda, 1.0\lambda)$. This figure confirms that Eq. (3) correctly compensates for the scattered waveform distortions. The computational time of this method is within 5.0 msec for each antenna location with a Xeon 3.2 GHz processor, which does not spoil the high-speed of the shape estimation.

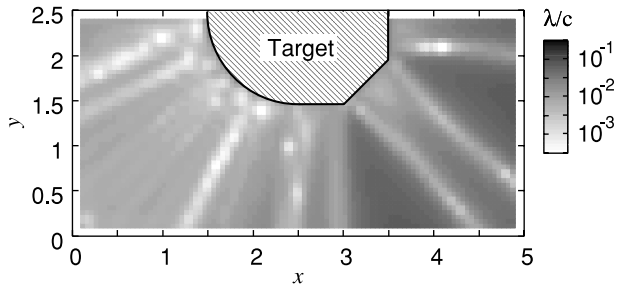

Fig. 6 Error of quasi wavefront with the transmitted waveform.

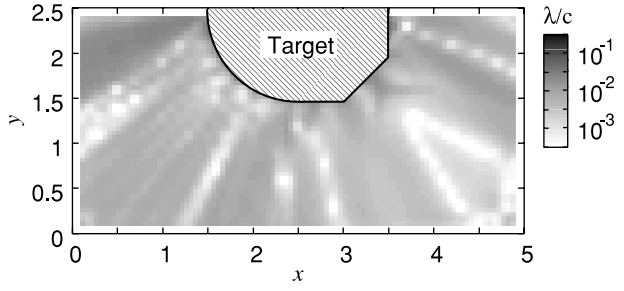

Fig. 7 Error of quasi wavefront with the estimated waveform.

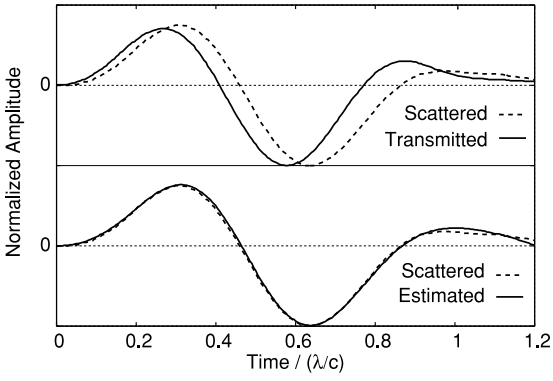

Fig. 8 Examples of the scattered and estimated waveforms.

5.2 Examples of Shape Estimation with Numerical Simulations

In this section, we verify the effectiveness of the proposed method with numerical simulations as follows. The left and right side of Fig. 9 show the output of the matched filter and the quasi wavefront with each method. $\epsilon = 0.01\lambda$ is set empirically, and the number of the iteration is 4. The proposed method accomplishes the 5 times improvement for the accuracy of the quasi wavefront than the conventional method. Figure 10 shows the estimated image with the proposed method. The target boundary, including the edges, is expressed more accurately compared to Fig. 3. This is because the estimated quasi wavefront is close to the true one with the proposed method. In addition, the estimated accuracy at the edge is within 0.01λ, which is 7 times more accurate than the conventional method.

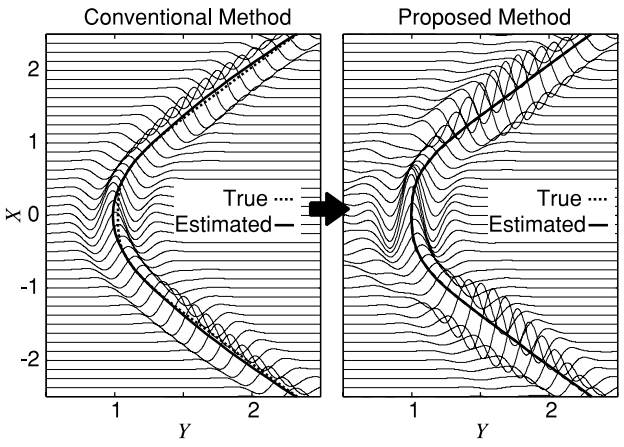

Fig. 9 Output of the filter and extracted quasi wavefront with each method.

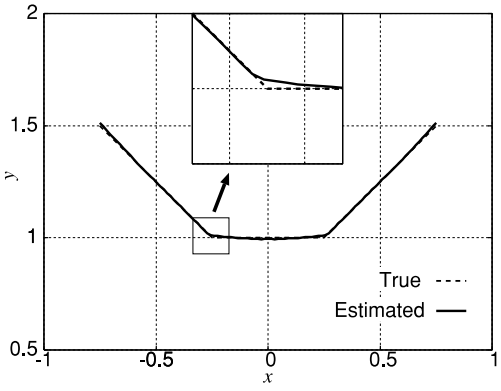

Fig. 10 Estimated image with the proposed method.

Furthermore, let us evaluate a curvature of the target boundary, which is expressed as

$$\kappa = \frac{\mathrm{d}^2y/\mathrm{d}x^2}{(1 + (\mathrm{d}y/\mathrm{d}x)^2)^{3/2}}. \tag{10}$$

Here a difference approximation is used to calculate $\mathrm{d}y/\mathrm{d}x$ and $\mathrm{d}^2y/\mathrm{d}x^2$. Figure 11 shows the estimated curvature with each method. This figure shows that the curvature of the conventional method is not accurate for the edges. On the contrary, the estimated κ with the proposed method is more accurate, and we see the two edges clearly.

Next, we discuss the estimation accuracy in a noisy environment. We introduce the evaluation value μ as

$$\mu = \frac{\sqrt{\int_{x_{\min}}^{x_{\max}} \{f_{\mathrm{t}}(x) - f_{\mathrm{e}}(x)\}^2 \mathrm{d}x}}{\sqrt{\int_{x_{\min}}^{x_{\max}} f_{\mathrm{t}}(x)^2 \mathrm{d}x}} \tag{11}$$

where $f_{\mathrm{t}}(x)$ and $f_{\mathrm{e}}(x)$ are the true and estimated target boundary, respectively, and $x_{\min}$ and $x_{\max}$ are minimum and maximum x for the estimated boundary. Figure 12 shows μ of the estimated boundary to S/N ratio. Also we define S/N as

$$\mathrm{S/N} = \frac{1}{\sigma_{\mathrm{N}}^2 (X_{\max} - X_{\min})} \int_{X_{\min}}^{X_{\max}} \max_{Y} |s(X, Y)|^2 \mathrm{d}X, \tag{12}$$

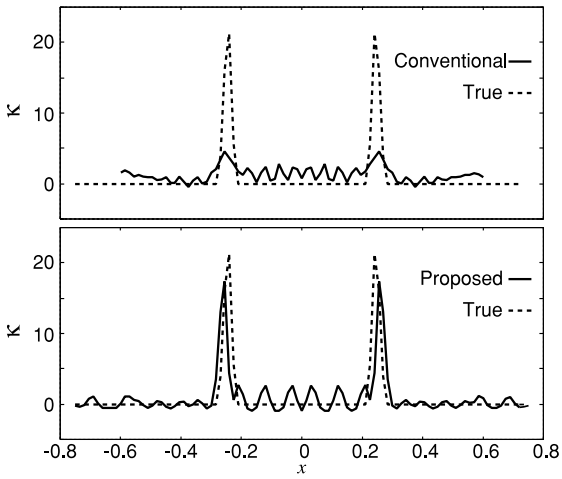

Fig. 11 Estimated curvature with the conventional (Upper) and the proposed methods (Lower).

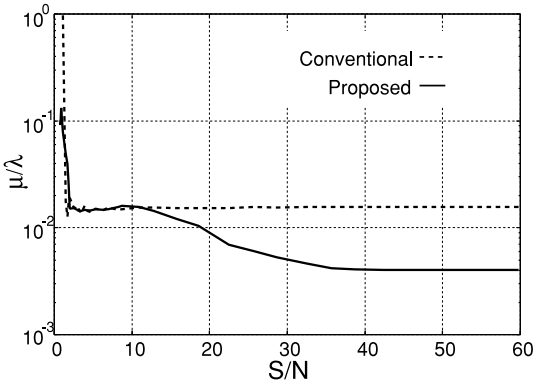

Fig. 12 Estimation accuracy of the estimated image for S/N.

where σ_{N} is a standard deviation of the noise. As shown in this figure, the 6 times improvement is obtained for the accuracy compared to the conventional method for S/N $\geq$ 30 dB. It also confirms us that the proposed method is effective for S/N $\geq$ 20 dB. These conditions are quite realistic because we utilize coherent averaging for radar systems.

Furthermore, we examine examples in the case of the target with both smooth curves and an edge. Figures 13 and 14 show the estimated image with the conventional method and the proposed method, respectively. As shown in these figures, a more accurate image can be obtained around the edges and the smooth curve of the target. These results show that the proposed method can be applied to a general curved target. The calculation time for this method is 2.0 sec with Xeon 3.2 GHz processor.

5.3 Examples of Shape Estimation with Experiments

In this section, let us investigate the performance of our algorithm with the experiments. We utilize the UWB pulses with the center frequency of 3.3 GHz and the 10 dB bandwidth of 2.0 GHz. The antenna has an elliptic polarization whose ratio of the major to the minor axis is about 17 dB,

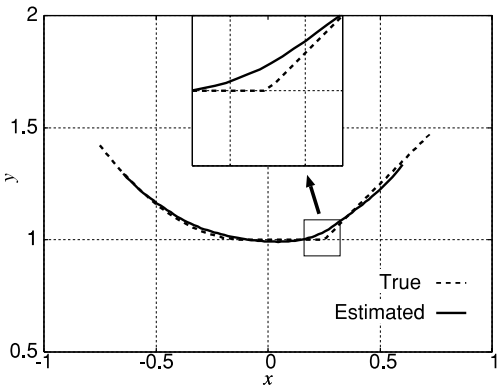

Fig. 13 Estimated image with the conventional method for the curved target.

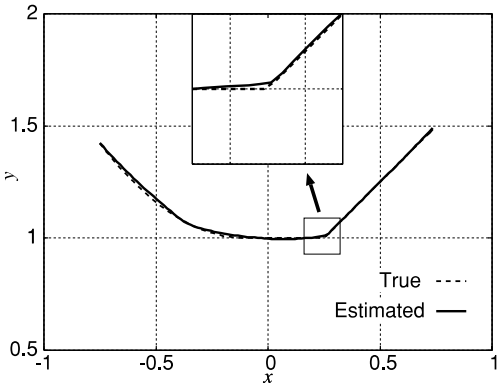

Fig. 14 Estimated image with the proposed method for the curved target.

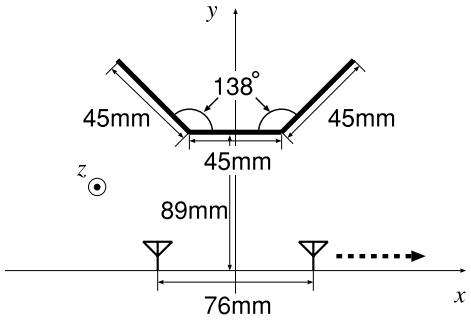

Fig. 15 Arrangement of bi-static antennas and targets in experiments.

and the direction of the polarimetry axis of the antenna is along the z axis. The 3 dB-beamwidth of the antenna is about 90°. The target is made of stainless steel sheet. Figure 15 illustrates the location of the antenna and the target. We utilize two antennas whose separation in x-direction is 76 mm, which corresponds to 0.835 center wavelength of 91 mm. The antenna location $(X, 0, 0)$ is defined as the center point of the two antennas. The target is set with a sufficiently long span in the z direction, compared to the center wavelength in order to obtain the data for the 2-dimensional problem. Additionally, the multiple scattered waveforms are integrated with a common midpoint for fixed $(X, 0, 0)$ [8]. Figure 16 shows the arrangement of the pair antennas and

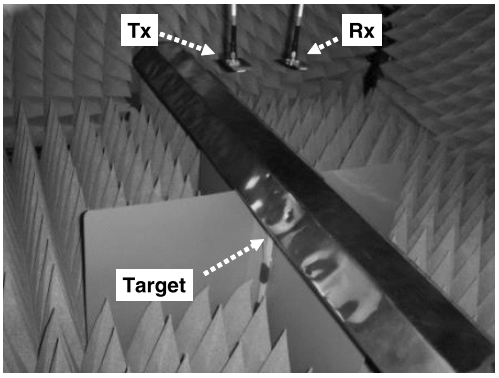

Fig. 16 Arrangement of the pair antenna and the target in experiments.

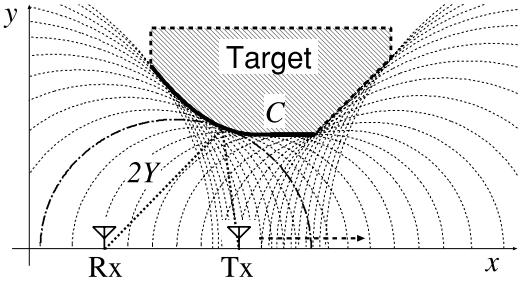

Fig. 17 Target boundary and an envelope of the ellipses for bi-static model.

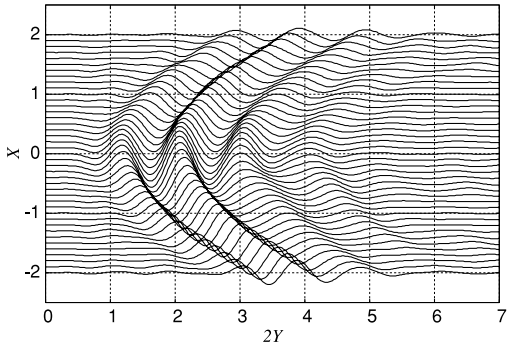

Fig. 18 Scattered waveforms in experiments.

the target in real environment. The data is coherently averaged 1024 times to enhance the S/N. The antenna pair are scanned for the range of $-200\,\text{mm} \leq x \leq 200\,\text{mm}$ where the sampling interval is set to 10 mm. We first measure the direct-wave without scattering, and eliminate the direct-waveform from the received signals to obtain the scattered waveform.

The proposed method can be easily extended to the bi-static system. In the bi-static model, the target boundary is estimated with the envelope of the ellipses which utilize the location of the transmitted and received antenna as the focus. Figure 17 illustrates the envelope of the ellipses for the antenna pair. We also easily extend the scattered waveform estimation to the pair antennas with setting an integral path for the two-path model as shown in Fig. 17. Figure 18 shows the

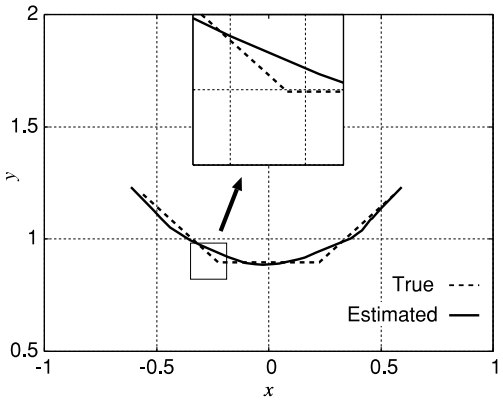

Fig. 19 Estimated image with the conventional method in experiments.

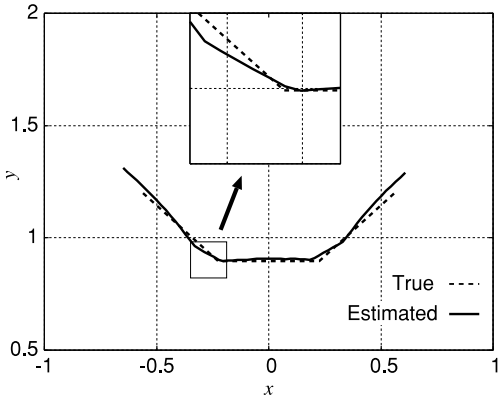

Fig. 20 Estimated image with the proposed method in experiments.

observed signals with our experiment. The S/N is 35.0 dB. Figures 19 and 20 show the estimated images with the conventional and the proposed method, respectively. The number of iterations is 5. As shown in Fig. 19, the estimated image does not have sufficient resolution around the edges, and μ of this image is about $2.2 \times 10^{-2}\lambda$. In contrast, the image with the proposed method is more accurate than the conventional method, especially around the edges. μ of this image is about $1.5 \times 10^{-2}\lambda$. Figure 21 shows the estimated curvature with each method. This figure shows that the proposed method can accurately estimate the locations of the edges. However, there are two false peaks of the curvature for the proposed method, and the image around the edges deteriorates compared with Fig. 10. These false peaks are caused by the small errors of the quasi wavefront. This is because we cannot completely eliminate the direct wave and the undesirable echoes from other objects. The cables and the plastic poles which support the antennas contribute to the received signal as the multiple scattered wave between the target and those objects. Additionally, these false peaks are also estimated in numerical simulations, where we add the white noise (S/N = 20 dB) as shown in Fig. 22. Therefore, data with higher S/N and S/I is needed to enhance the accuracy of this region.

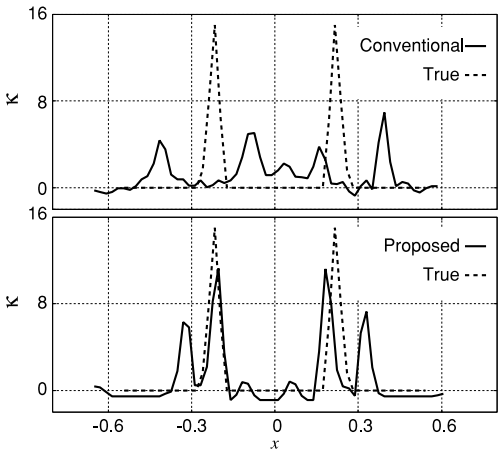

Fig. 21 Estimated curvature with the conventional (Upper) and the proposed (Lower) methods in experiments.

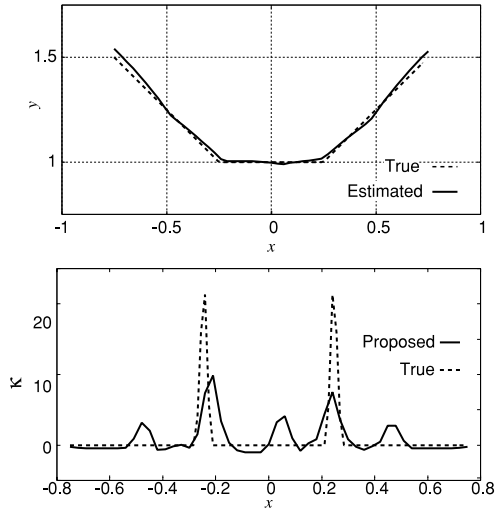

Fig. 22 Estimated image with the proposed method in numerical simulations for S/N=20 dB (Upper) and estimated curvature (Lower).

6. Conclusion

We proposed a high-resolution imaging algorithm by simultaneously estimating the shape and scattered waveform. It is clarified that the proposed method achieves a high-resolution imaging and correctly identifies the characteristic of the target shape. The accuracy of the estimated image is better than 0.01λ, with a numerical simulation for $S/N \geq 19$ dB. We have investigated the performance of the proposed method with the experiments, and clarify the effectiveness of the method in detecting edges even for the realistic environment.

Acknowledgment

We thank Dr. Satoru Kurokawa at Advanced Industrial Science and Technology, Japan, and Mr. Satoshi Sugino at National Institute of the New Product Technologies Development Department, Matsushita Electric Works, Ltd, Japan for their valuable advices. This work is supported in part by the 21st Century COE Program (Grant No. 14213201).

References

[1] C. Chiu, C. Li, and W. Chan, "Image reconstruction of a buried conductor by the genetic algorithm," IEICE Trans. Electron., vol.E84-C, no.12, pp.1946–1951, Dec. 2001.
[2] T. Takenaka, H. Jia, and T. Tanaka, "Microwave imaging of an anisotropic cylindrical object by a forward-backward time-stepping method," IEICE Trans. Electron., vol.E84-C, no.12, pp.1910–1916, Dec. 2001.
[3] T. Sato, K. Takeda, T. Nagamatsu, T. Wakayama, I. Kimura, and T. Shinbo, "Automatic signal processing of front monitor radar for tunneling machines," IEEE Trans. Geosci. Remote Sens., vol.35, no.2, pp.354–359, 1997.
[4] T. Sato, T. Wakayama, and K. Takemura, "An imaging algorithm of objects embedded in a lossy dispersive medium for subsurface radar data processing," IEEE Trans. Geosci. Remote Sens., vol.38, no.1, pp.296–303, 2000.
[5] T. Sakamoto and T. Sato, "A target shape estimation algorithm for pulse radar systems based on boundary scattering transform," IEICE Trans. Commun., vol.E87-B, no.5, pp.1357–1365, May 2004.
[6] T. Sakamoto and T. Sato, "A phase compensation algorithm for high-resolution pulse radar systems," IEICE Trans. Commun., vol.E87-B, no.6, pp.1631–1638, June 2004.
[7] S. Kidera, T. Sakamoto, and T. Sato, "A robust and fast imaging algorithm with an envelope of circles for UWB pulse radars," IEICE Trans. Commun., vol.E90-B, 2007, (To be published).
[8] S. Kidera, T. Sakamoto, T. Sato, and S. Sugino, "An accurate imaging algorithm with scattered waveform estimation for UWB pulse radars," IEICE Trans. Commun., vol.E89-B, no.9, pp.2588–2595, Sept. 2006.

Shouhei Kidera received the B.E. degree from Kyoto University in 2003 and the M.I. degree at Graduate School of Informatics, Kyoto University in 2005. He is currently studying for the Ph.D. degree at Graduate School of Informatics, Kyoto University. His current research interest is in signal processing for UWB pulse radars. He is a member of the IEEE.

Takuya Sakamoto was born in Nara, Japan in 1977. Dr. Sakamoto received his B.E. degree from Kyoto University in 2000, and his M.I. and Ph.D. degrees from Graduate School of Informatics, Kyoto University in 2002 and 2005, respectively. He is a research associate in the Department of Communications and Computer Engineering, Graduate School of Informatics, Kyoto University. His current research interest is in signal processing for UWB pulse radars. He is a member of the IEEJ and the IEEE.

Toru Sato received his B.E., M.E., and Ph.D. degrees in electrical engineering from Kyoto University, Kyoto, Japan in 1976, 1978, and 1982, respectively. He has been with Kyoto University since 1983 and is currently a Professor in the Department of Communications and Computer Engineering, Graduate School of Informatics. His major research interests have been system design and signal processing aspects of atmospheric radars, radar remote sensing of the atmosphere, observations of precipitation using radar and satellite signals, radar observation of space debris, and signal processing for subsurface radar signals. Dr. Sato was awarded Tanakadate Prize in 1986. He is a member of the Society of Geomagnetism and Earth, Planetary and Space Sciences, the Japan Society for Aeronautical and Space Sciences, the Institute of Electrical and Electronics Engineers, and the American Meteorological Society.